C-Band Dual-Polarization Radar Observables in Rain

K. AYDIN AND V. GIRIDHAR

Department of Electrical and Computer Engineering, The Pennsylvania State University, University Park, Pennsylvania

(Manuscript received 1 April 1991, in final form 21 October 1991)

ABSTRACT

C-band dual-linear polarization radar observables are simulated from disdrometer measurements in rainfall and from gamma-model raindrop-size distributions. It is shown that rainfall is clustered in certain sections of planes formed by selected pairs of radar observables, such as (Z_H, Z_{DR}), (Z_H, Z_{DP}), (Z_H, K_{DP}), and (ρ, Z_{DR}). Measurements lying outside these rainfall cluster regions can be interpreted as being from ice- and mixed-phase hydrometeors. Relationships for estimating rainfall rate R from radar measurements of Z_H, K_{DP}, and (Z_H, Z_{DR}) are derived, and the latter is shown to produce the best results. An important problem for C-band measurements in the presence of rainfall is attenuation. For this purpose, relationships are derived for estimating specific attenuation and specific differential attenuation from the specific differential phase. The backscattering differential phase shift, which is a potential source of error in estimating K_{DP}, is shown to be very sensitive to the drop-size distribution. The effects of raindrop temperature and canting on the derived relationships are discussed. Finally, S-band relations similar to those obtained at C band are also presented.

1. Introduction

The utility of dual-linear polarization radars for estimating rain rate, detecting hail, and differentiating hydrometeor phase (liquid water and ice) has been demonstrated by numerous studies published in journals and presented in radar meteorology conferences during the last decade (for an extensive list of references see Atlas 1990). Most of these studies have focused on S-band (10-cm wavelength) radars. In Europe, an increasing number of polarimetric C-band (5-cm wavelength) meteorological radars are being tested for research and operational purposes, as in Germany and in Italy, where one is incorporated in the Arno project (a project for flash-flood forecasting in the Arno River basin). Hence, there is a growing need for better understanding the utility of various polarimetric radar observables at C band.

This paper presents simulations of C-band polarimetric radar observables based on disdrometer measurements and gamma-model raindrop-size distributions. Several relations between these observables are proposed for differentiating hydrometeor phase. Equations useful in estimating rainfall rate from the effective reflectivity factor at horizontal polarization Z_H, specific differential phase K_{DP}, and Z_H and Z_{DR} (differential reflectivity) are presented both at C-band and S-band wavelengths. Relations between the specific attenuation and K_{DP} are derived for use in attenuation correction of radar observables. Raindrop water temperature is shown to significantly affect these relations. Finally, the backscattering differential phase shift, which is a potential error source for the estimate of K_{DP}, is shown to be very sensitive to the drop-size distribution as well as the raindrop temperature. The effects of raindrop canting on the aforementioned parameters are also discussed.

2. Radar observables simulated from disdrometer measurements

The disdrometer measurements of raindrop-size distributions used in this study were obtained near Boulder, Colorado, during the months of May and June in 1983 and 1984, and in central Illinois in the fall of 1982 during convective and stratiform rainfall (Seliga et al. 1984, 1986; Aydin et al. 1987). The data were recorded every 30 s and later smoothed by performing 2-min running averages. Only those distributions with $R > 0.5$ mm h^{-1} and with more than 100 drops were considered, resulting in 1036 drop-size distributions. The C-band radar observables presented here were simulated from these measurements at a wavelength of 5.4 cm and raindrop temperatures of 0°, 5°, 10°, and 20°C, corresponding to complex dielectric constants of 64.87-j37.33, 68.38-j33.45, 70.72-j29.57, and 72.68-j22.60, respectively (Ray 1972). The 10°C results are given and compared with those at the other temperatures.

Also, selected results at S band (10.9-cm wavelength) are presented for comparison with those at C band in the Appendix. Since the effects of temperature on radar

Corresponding author address: Dr. Kültegin Aydin, Pennsylvania State University, Communications and Space Sciences Lab, 316 Electrical Engineering East, University Park, PA 16802.

observables at S band are negligibly small, only the 10°C raindrop temperature is considered.

In this study, raindrops were modeled as oblate spheroids with Green's (1975) axial ratio and no canting. The effects of canting are discussed in section 2e. The electromagnetic-scattering computations were performed using the T-matrix formulation of Waterman (1969).

a. *Clustering of radar observables*

The clustering of C-band polarimetric radar observables in various planes of selected pairs may be useful in identifying the presence of different phase hydrometeors. Figure 1a shows the clustering in the Z_H–Z_{DR} plane due to rainfall at 10°C raindrop temperature. Since the data points corresponding to the upper Z_H bound in this cluster are almost the same as at S band, the differential reflectivity hail signal H_{DR} derived by Aydin et al. (1986) can also be used at C band:

$$H_{DR} = Z_H - f(Z_{DR}) \quad \text{(dB)}, \tag{1}$$

where

$$f(Z_{DR}) = \begin{cases} 27\ \text{(dBZ)} & Z_{DR} < 0\ \text{dB} \\ 19Z_{DR} + 27\ \text{(dBZ)} & 0\ \text{dB} \leq Z_{DR} \leq 1.74\ \text{dB} \\ 60\ \text{(dBZ)} & Z_{DR} > 1.74\ \text{dB}. \end{cases} \tag{2}$$

Here $H_{DR} > 0$ dB is proposed as an indicator of hail, as demonstrated by Aydin et al. (1986) at S band, who compared radar and in situ observations in Colorado hailstorms. The dashed curves in Fig. 1a serve as references based on the drop-size distribution of Marshall and Palmer (1948) with maximum drop sizes of 6 and 8 mm. It is worth noting that the expression in (2) is negligibly affected by raindrop temperature between 0° and 20°C.

Figure 1b shows the scatterplot of Z_H versus K_{DP} at 10°C raindrop temperature, illustrating a cluster pat-

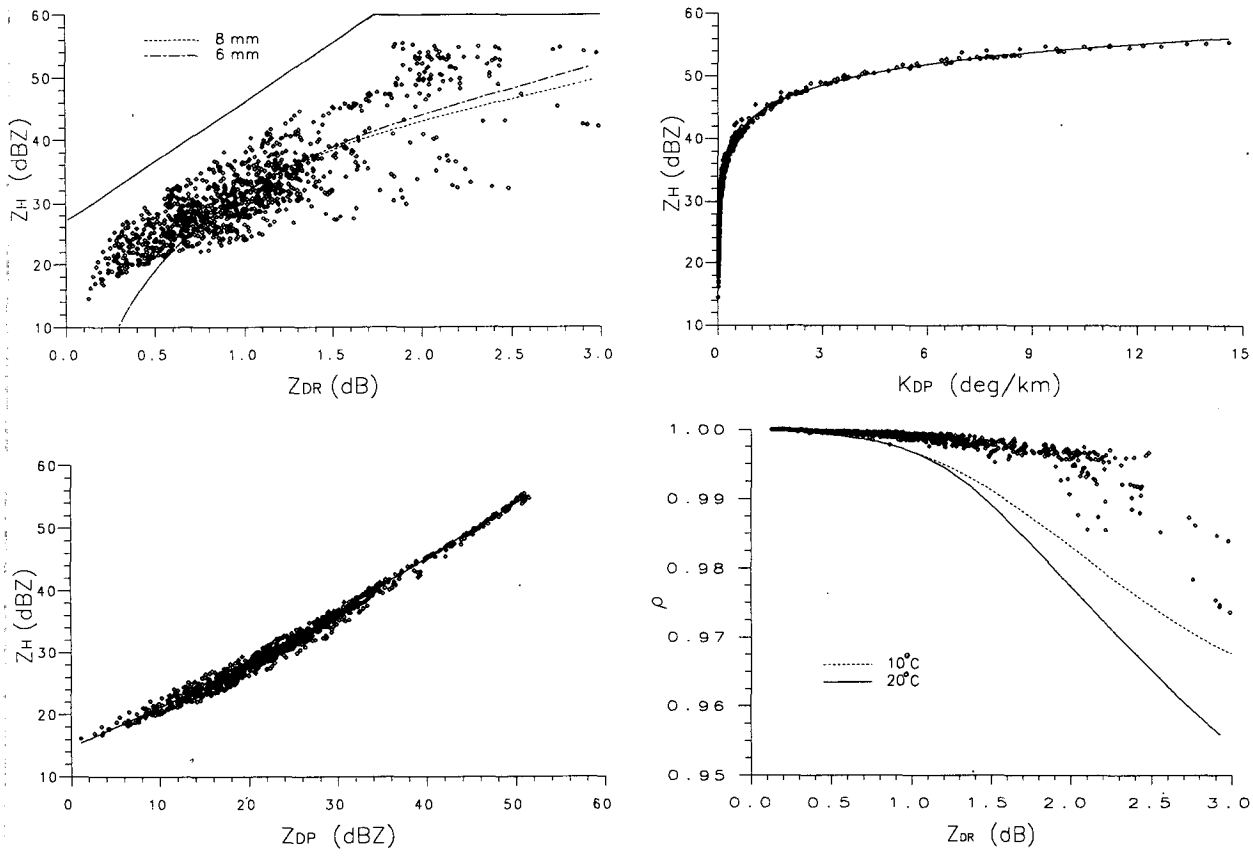

FIG. 1. Scatterplots of various C-band radar observables at 10°C raindrop temperature simulated from disdrometer measurements of raindrop-size distributions. (a) Z_H versus Z_{DR}; the solid curve corresponds to the upper bound of Z_H in rainfall (2), the dashed curves correspond to the Marshall–Palmer (1948) DSD with D_{max} = 6 and 8 mm; (b) Z_H versus K_{DP}, the best-fit curve (3) is also shown; (c) Z_H versus Z_{DP}, the best-fit curve (5) is also shown; (d) ρ versus Z_{DR}, the dashed (10°C) and solid (20°C) curves correspond to (6).

tern that is highly concentrated around the curve obtained by a least-squares fit to Z_H (dBZ) and $\log(K_{DP})$:

$$Z_H\,(\mathrm{dBZ}) = \begin{cases} 12.04\log(K_{DP}) + 43.77 \\ \qquad 0.01 < K_{DP}\,(^\circ\ \mathrm{km}^{-1}) < 0.15 \\ 11.03\log(K_{DP}) + 43.3 \\ \qquad 0.15 \leq K_{DP}\,(^\circ\ \mathrm{km}^{-1}) < 15, \end{cases} \tag{3}$$

where K_{DP} is the one-way specific differential phase. Significant deviations from this curve should indicate the presence of hydrometeors other than raindrops. Note that changes in raindrop temperature between 0° and 20°C have very little effect on (3). For a given value of K_{DP} the relation in (3) yields a slightly higher value of Z_H (dBZ) at 0°C and a slightly lower value at 20°C, producing a change less than 1% in both cases. An expression similar to (3) was derived by Balakrishnan and Zrnić (1990) at S band. The S-band result corresponding to (3) is given in the Appendix.

Figure 1c shows the clustering of (Z_H, Z_{DP}) pairs in rainfall at 10°C raindrop temperature, where the difference reflectivity $Z_{DP} = 10\log(Z_H - Z_V)$ for $Z_H > Z_V$ ($\mathrm{mm}^6\ \mathrm{m}^{-3}$) (Golestani et al. 1989). This definition can be generalized to include measurements with $Z_H < Z_V$, which is possible in hail and other ice forms:

$$Z_{DP}\,(\mathrm{dBZ}) = 10\log(|Z_H - Z_V|). \tag{4}$$

A least-squares fit to the data in Fig. 1c yields

$$Z_H\,(\mathrm{dBZ}) = \begin{cases} 0.64Z_{DP} + 14.73 & 1 < Z_{DP}\,(\mathrm{dBZ}) \leq 20 \\ 0.87Z_{DP} + 10.1 & 20 < Z_{DP}\,(\mathrm{dBZ}) < 52. \end{cases} \tag{5}$$

The standard deviation of Z_H around this curve is less than 0.9 dBZ. Therefore, significant deviations of Z_H from (5), for example, 3 dBZ or more, as well as negative values of Z_{DP}, may be interpreted as being due to ice- or mixed-phase precipitation. Note that the relationship in (5) is not affected by raindrop temperature between 0° and 20°C.

Figure 1d shows the scatterplot of ρ versus Z_{DR} in rainfall at 10°C raindrop temperature, where ρ denotes the magnitude of the zero-lag cross correlation between copolar H and V echoes. It is seen that $\rho > .99$ for $Z_{DR} < 2$ dB and $\rho > .996$ for $Z_{DR} < 1.5$ dB. The curves shown in this figure correspond to a lower limit on ρ at 10° and 20°C raindrop temperatures obtained from a gamma-model drop-size distribution $[N(D) = N_0 D^m e^{-\Lambda D}]$ with $m = 0$ and $D_{max} = 8$ mm. Other model results are shown in Fig. 2. The models illustrate the sensitivity of ρ on the maximum raindrop size, which is limited to 5.5 mm in the disdrometer measurements. This sensitivity can be attributed to the significant variation in the backscattering differential phase shift for raindrops with $D > 5$ mm (see section 2d). It is clear from Fig. 2b that the ρ–Z_{DR} relation is also very sensitive to raindrop temperature. The equations for the curves shown in Fig. 1d are

$$\rho = 1.00052 - 0.00448Z_{DR} + 0.00850Z_{DR}^2 - 0.01070Z_{DR}^3 + 0.00333Z_{DR}^4 - 0.00032Z_{DR}^5 \quad (10^\circ\mathrm{C}) \tag{6a}$$

and

$$\rho = 1.00092 - 0.00769Z_{DR} + 0.01675Z_{DR}^2 - 0.01835Z_{DR}^3 + 0.00557Z_{DR}^4 - 0.00054Z_{DR}^5 \quad (20^\circ\mathrm{C}). \tag{6b}$$

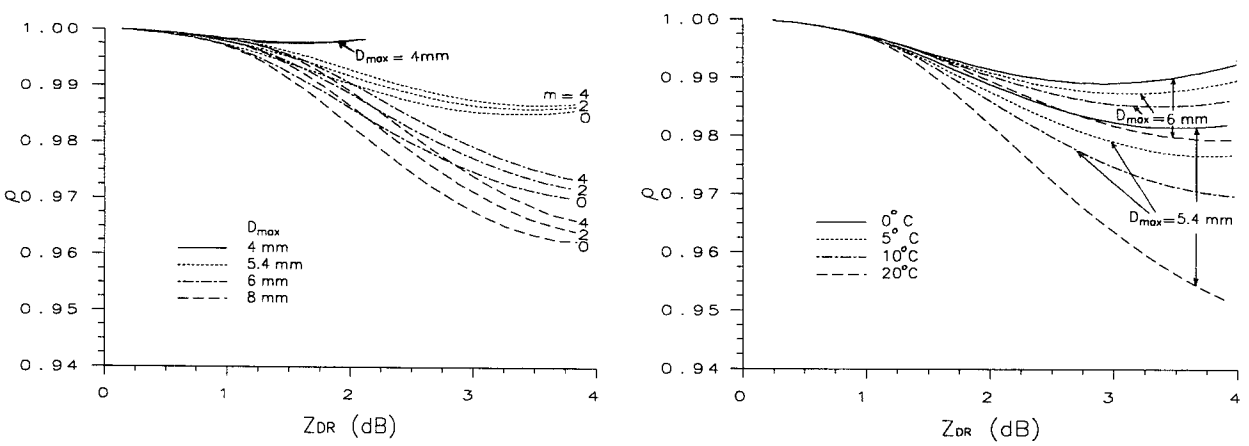

FIG. 2. Magnitude of C-band zero-lag cross correlation as a function of Z_{DR} based on gamma-model raindrop-size distributions $[N(D) = N_0 D^m e^{-\Lambda D}]$ with maximum drop diameter D_{max}: (a) dependence on model parameters at 10°C raindrop temperature and (b) raindrop-temperature dependence based on gamma-model DSDs with $m = 0$.

Measured pairs of (ρ, Z_{DR}) falling below the 20°C curve (6b) could indicate that the radar returns are not from pure rain.

It is worth noting that radar observations of precipitation other than pure rain may very well produce similar signatures as rainfall. However, by using several different radar observables, this possibility may be significantly reduced.

b. *Rainfall-rate estimation*

It has been demonstrated by a significant number of measurements (see, e.g., Aydin et al. 1987, 1990 and the references cited therein) that the pair (Z_H, Z_{DR}) provides improved estimates of rainfall rate R compared to simply using Z_H alone (Seliga and Bringi 1976). All of these experiments have been performed with S-band radars. Similar results are expected at C band, assuming that the Z_H and Z_{DR} measurements are corrected for attenuation. A relationship between R and (Z_H, Z_{DR}) at 10°C raindrop temperature, obtained through a two-parameter least-squares fit, is

$$R = 2.37 \times 10^{-3} Z_H^{0.95} Z_{DR}^{-1.17} \quad (\text{mm h}^{-1}), \quad (7)$$

where Z_H ranges from $10^{1.5}$ to $10^{5.6}$ mm^6 m^{-3} and Z_{DR} ranges from 0.1 to 3 dB. This equation is almost identical to that derived by Aydin et al. (1989) using the same database and including $R < 0.5$ mm h^{-1}. The corresponding relationship at S band is given in the Appendix. The biases in the rainfall rates estimated from (7) for R in the ranges 0.5–2, 2–5, 5–50, 50–218 mm h^{-1} are 2%, −1%, −1%, and 1% (where positive values imply overestimation by radar), and the corresponding standard errors are 10%, 9%, 7%, and 3%. The effect of raindrop temperature between 0° and 20°C on (7) is very small; that is, the errors in estimating R from (7) in place of the 0° and 20°C equations are less than 2% and 4%, respectively.

Another technique for estimating rainfall rate is through an R–K_{DP} relationship, which has been suggested for S-band radars (Sachidananda and Zrnić 1986; Chandrasekar et al. 1990). Figure 3 shows R versus K_{DP} at C band. The curve obtained from a least-squares fit to log$R$ and logK_{DP} at 10°C raindrop temperature is

$$R = \begin{cases} 18.45 K_{DP}^{0.82} \ (\text{mm h}^{-1}) & 0.01 < K_{DP} \ (^\circ \text{km}^{-1}) < 3 \\ 16.03 K_{DP}^{0.95} \ (\text{mm h}^{-1}) & 3 \leq K_{DP} \ (^\circ \text{km}^{-1}) < 15. \end{cases} \quad (8)$$

This relationship produces the following biases in R for the ranges 0.5–2, 2–5, 5–50, 50–218 mm h^{-1}: 8%, 0.1%, −3%, and −0.4%. The corresponding standard errors are: 29%, 21%, 12%, and 6%. Note that although the biases in R produced by (7) and (8) are comparable, the standard errors of (7) are significantly lower than those of (8). The effect of raindrop temperature between 0° and 20°C on (8) is also very small, causing less than 3% and 2% errors in R when compared with the 0° and 20°C equations, respectively. For a given K_{DP}, the estimated R tends to be slightly larger at higher temperatures. The S-band relationship corresponding to (8) is not temperature sensitive and is given in the Appendix.

An R–Z_H relationship was also derived from the same database at 10°C raindrop temperature:

$$R = \begin{cases} 0.08 Z_H^{0.452} \ (\text{mm h}^{-1}) \\ \qquad 10^{1.5} \leq Z_H \ (\text{mm}^6 \ \text{m}^{-3}) < 10^3 \\ 0.009 Z_H^{0.765} \ (\text{mm h}^{-1}) \\ \qquad 10^3 \leq Z_H \ (\text{mm}^6 \ \text{m}^3) < 10^{5.6}. \end{cases} \quad (9)$$

The biases in R from (9) for the ranges 0.5–2, 2–5, 5–50, 50–218 mm h^{-1} are 15%, −9%, −3%, and −6%. The corresponding standard errors are 38%, 32%, 23%, and 17%. This relationship does not perform as well as (7) and (8). However, the effect of raindrop temperature between 0° and 20°C on (9) is also small. The error in estimating R from (9) in place of the 0° or 20°C equations is less than 5%. The error tends to be lower for smaller R.

c. *Attenuation effects*

Most of the aforementioned radar observables at C band are affected by attenuation due to rain. Hence, unless they are corrected for the two-way attenuation, errors will arise in the radar estimates of rainfall parameters and in their interpretation for discriminating hydrometeor phase. An attenuation correction scheme based on estimating the specific attenuations A_H and A_V using Z_H and Z_{DR} was studied by Aydin et al. (1989). Another approach for attenuation correction

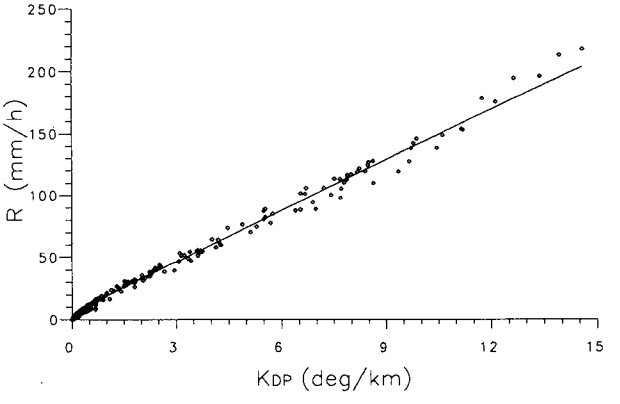

FIG. 3. Scatterplot of R versus K_{DP} (C band) at 10°C raindrop temperature obtained from disdrometer measurements in rain. The solid curve corresponds to (8).

makes use of K_{DP} (Bringi et al. 1990). Figure 4 shows the scatterplots of A_H and ΔA_{HV} (where $\Delta A_{HV} = A_H - A_V$) versus K_{DP}. A least-squares fit to $\log A$ and $\log K_{DP}$ (where A is A_H or A_V or ΔA_{HV}) produces the following power-law relationships at 10°C raindrop temperature:

$$A_H = \begin{cases} 0.060 K_{DP}^{0.94} \text{ (dB km}^{-1}\text{)} \\ \qquad 0.01 < K_{DP} (^\circ \text{ km}^{-1}) < 1 \\ 0.059 K_{DP}^{1.07} \text{ (dB km}^{-1}\text{)} \\ \qquad 1 \leq K_{DP} (^\circ \text{ km}^{-1}) < 15 \end{cases} \quad (10)$$

$$A_V = \begin{cases} 0.047 K_{DP}^{0.9} \text{ (dB km}^{-1}\text{)} \\ \qquad 0.01 < K_{DP} (^\circ \text{ km}^{-1}) < 1 \\ 0.046 K_{DP}^{1.02} \text{ (dB km}^{-1}\text{)} \\ \qquad 1 \leq K_{DP} (^\circ \text{ km}^{-1}) < 15 \end{cases} \quad (11)$$

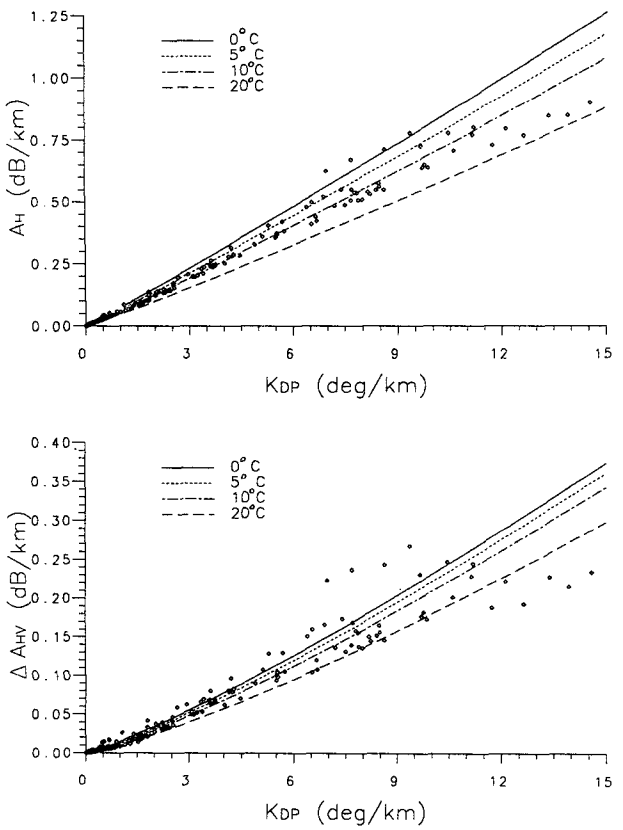

FIG. 4. Scatterplot of C band (a) A_H and (b) ΔA_{HV} versus K_{DP}, simulated at 10°C raindrop temperature from disdrometer measurements in rain. The best-fit curves (10) and (12) are shown by the 10°C lines. The other curves are for 0°, 5°, and 20°C raindrop temperatures.

$$\Delta A_{HV} = 0.0126 K_{DP}^{1.22} \text{ (dB km}^{-1}\text{)} \quad 0.01 < K_{DP} (^\circ \text{ km}^{-1}) < 15. \quad (12)$$

The biases produced by (10) and (11) for A_H and A_V in the ranges 0.001–0.1, 0.1–0.3, and 0.3–0.9 dB km^{-1} are 4%, −1%, and 1%. The corresponding standard errors for (10) are 20%, 6%, and 11%, and for (11) are 13%, 3%, and 6%. The biases produced in ΔA_{HV} by (12) in the ranges 0.0003–0.03, 0.03–0.1, and 0.1–0.27 dB km^{-1} are 1%, −7%, and 2%, and the corresponding standard errors are 73%, 13%, and 24%. An important problem that might arise in using these equations is that the estimate of K_{DP} may be in error due to the backscattering differential phase shift, which is discussed in the next section.

The effects of raindrop temperature (between 0° and 20°C) on the relationships (10), (11), and (12) are significant, as illustrated in Fig. 4. It is seen that for a given K_{DP} the corresponding A_H and ΔA_{HV} decrease as the raindrop temperature increases from 0° to 20°C. The errors in estimating A_H from (10), compared to using the 0° and the 20°C equations, are from 17% to 24% and 23% to 26%, respectively. Similarly, using (12) instead of the 0° and 20°C equations for estimating ΔA_{HV} leads to errors from 9% to 18% and 14% to 26%, respectively. Note that the errors tend to be lower as both A_H and ΔA_{HV} increase. Since these errors are significant, it is worthwhile presenting the equations obtained at 0° and 20°C raindrop temperatures. In the relationship

$$A_H \text{ (or } A_V) = a K_{DP}^b \quad \text{(dB km}^{-1}\text{)} \quad (13)$$

the parameters (a, b) at 0°C are (0.073, 0.93) and (0.73, 1.05) for A_H, and (0.058, 0.88) and (0.58, 1.01) for A_V, corresponding to K_{DP} (° km^{-1}) in the ranges 0.01 to 1 and 1 to 15, respectively. Similarly, (a, b) at 20°C are (0.047, 0.95) and (0.047, 1.08) for A_H and (0.037, 0.9) and (0.036, 1.03) for A_V, corresponding to K_{DP} (° km^{-1}) in the ranges 0.01 to 1 and 1 to 15, respectively. Finally, for $0.01 < K_{DP}$ (° km^{-1}) < 15

$$\Delta A_{HV} = 0.0150 K_{DP}^{1.19} \quad \text{(dB km}^{-1}\text{)} \quad \text{at 0°C} \quad (14)$$

and

$$\Delta A_{HV} = 0.0102 K_{DP}^{1.25} \quad \text{(dB km}^{-1}\text{)} \quad \text{at 20°C.} \quad (15)$$

It is of interest to compare (10)–(15) with the linear relations derived by Bringi et al. (1990) at 15°C raindrop temperature, where $A_H = 0.054 K_{DP}$ and $\Delta A_{HV} = 0.0157 K_{DP}$ based on gamma-model simulations and $A_H = 0.05 K_{DP}$ and $\Delta A_{HV} = 0.0139 K_{DP}$ based on disdrometer measurements in Oklahoma. The A_H values from both of their equations compare best with our 20°C relation given in (13). Their gamma-model relation matches better (producing slightly lower values of A_H) when $K_{DP} > 3.5°$ km^{-1}, whereas their disdrometer relation is a better match when K_{DP}

$< 3.5°$ km^{-1}. Furthermore, both are closer to the 10°C equation given in (10) for $K_{DP} < 1°$ km^{-1}. On the other hand, (12), (14), and (15) are not linear relations between ΔA_{HV} and K_{DP} like those of Bringi et al. (1990). However, (15) matches best with their gamma-model relation for $K_{DP} > 4.5°$ km^{-1} and their disdrometer relation for $K_{DP} \leq 4.5°$ km^{-1}.

d. *Backscattering differential phase shift*

Equations (10)–(15) can produce reasonably accurate results for the attenuation if K_{DP} is itself accurate. Aside from measurement errors and errors due to gradients of the drop-size distribution (DSD) parameters in the radar resolution volume, K_{DP} can be affected by the spatial variation of the backscattering differential phase shift δ. Note that $K_{DP} = d\phi_{DP}/dr$, where ϕ_{DP} is the one-way propagation differential phase shift and r is the distance along the radar beam, and the estimate of ϕ_{DP} is composed of the actual propagation differential phase shift plus δ (Sachidananda and Zrnic 1986). At S-band wavelengths δ is negligibly small in rain (Jameson and Mueller 1985). However, as seen in Fig. 5, δ can become significant at C band. In fact, the sharp transition from negative values between D = 3.5–5.3 mm and large positive values for $D > 5.3$ mm shows that δ is very sensitive to the DSD parameters, especially the maximum drop size D_{max}. It is also clear from Fig. 5 that δ is significantly affected by raindrop temperature in this transition region. Figure 6a shows the scatterplot of δ versus Z_{DR} simulated from disdrometer measurements. The gamma-model [$N(D) = N_0 D^m e^{-\Lambda D}$] DSD results show a larger range of values for δ (Fig. 6b). One reason for this is that the maximum drop size registered by the disdrometer is 5.5 mm even if a drop has a larger diameter. The curves with D_{max} = 5.4 mm are very similar to the disdrometer results. However, when D_{max} is increased to 6 and 8 mm there is a dramatic shift in δ to large positive values. It is worth noting that Bringi et al. (1990) have also simulated δ at C band, based on gamma-model drop-size distribution, producing only positive values for δ. This is because D_{max} was set to 8 mm in their simulations. Their results are in good agreement with those in Fig. 6b for the same D_{max} value. Figure 6c illustrates the temperature dependence of δ versus Z_{DR} using gamma model DSDs. It is clear that for $Z_{DR} < 1.5$ dB δ is negligibly small. For $Z_{DR} > 1.5$ dB the effect of D_{max} and temperature on δ becomes very significant.

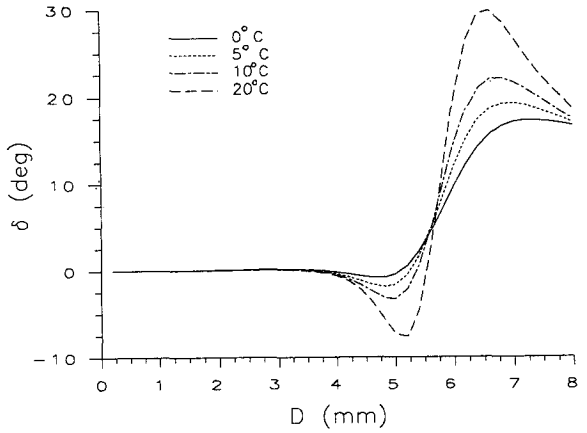

FIG. 5. C-band backscattering differential phase shift as a function of raindrop diameter D and for 0°, 5°, 10°, and 20°C raindrop temperatures.

e. *Effects of raindrop canting*

The effects of raindrop canting on the relations just discussed are illustrated using a simple canting model in which the canting angle is confined to the plane formed by the vertical (V) and horizontal (H) directions. The radar line of sight direction is assumed to be perpendicular to this plane. The canting angle α is defined as the angle between the symmetry axis of the oblate spheroidal raindrop and the V direction. A Gaussian canting angle distribution is used with mean value $\bar{\alpha} = 0°$ and standard deviation $\sigma_\alpha = 10°$.

The effect of canting on the relations (2), (3), and (5) is negligible, less than 1% difference in Z_H. Similarly, (6) is altered very little, less than 0.4%. The rain-rate relations (7), (8), and (9) are slightly affected. With canting, (7) overestimates R by 7%, (8) underestimates R by 6%, and the error in the estimate of R from (9) is within ±1%. Similarly, A_H and A_V are overestimated by 7% using (10) and (11), and the error in the estimate of ΔA_{HV} from (12) is within −8% to +6%. It is clear that the effects of raindrop temperature (0°–20°C) are more significant than canting ($\bar{\alpha} = 0°$, $\sigma_\alpha = 10°$) on all of these relations.

3. Summary and conclusions

C-band dual-linear polarization radar observables were simulated using ground-based disdrometer measurements of raindrop-size distributions. The effects of raindrop temperature and canting were considered. Other effects mainly related to radar measurements, such as estimation errors, radar beam filling, and reflectivity gradients, were not included. Rainfall data were shown to be clustered in specific regions of the Z_H–Z_{DR}, Z_H–K_{DP}, Z_H–Z_{DP}, and ρ–Z_{DR} planes. Data points lying outside these regions were proposed as indicators of hydrometeors other than pure rain, such as hail, graupel, snow, and mixed-phase precipitation. It is possible that such hydrometeors could produce similar signatures as pure rain, in which case their discrimination may be difficult. However, this possibility could

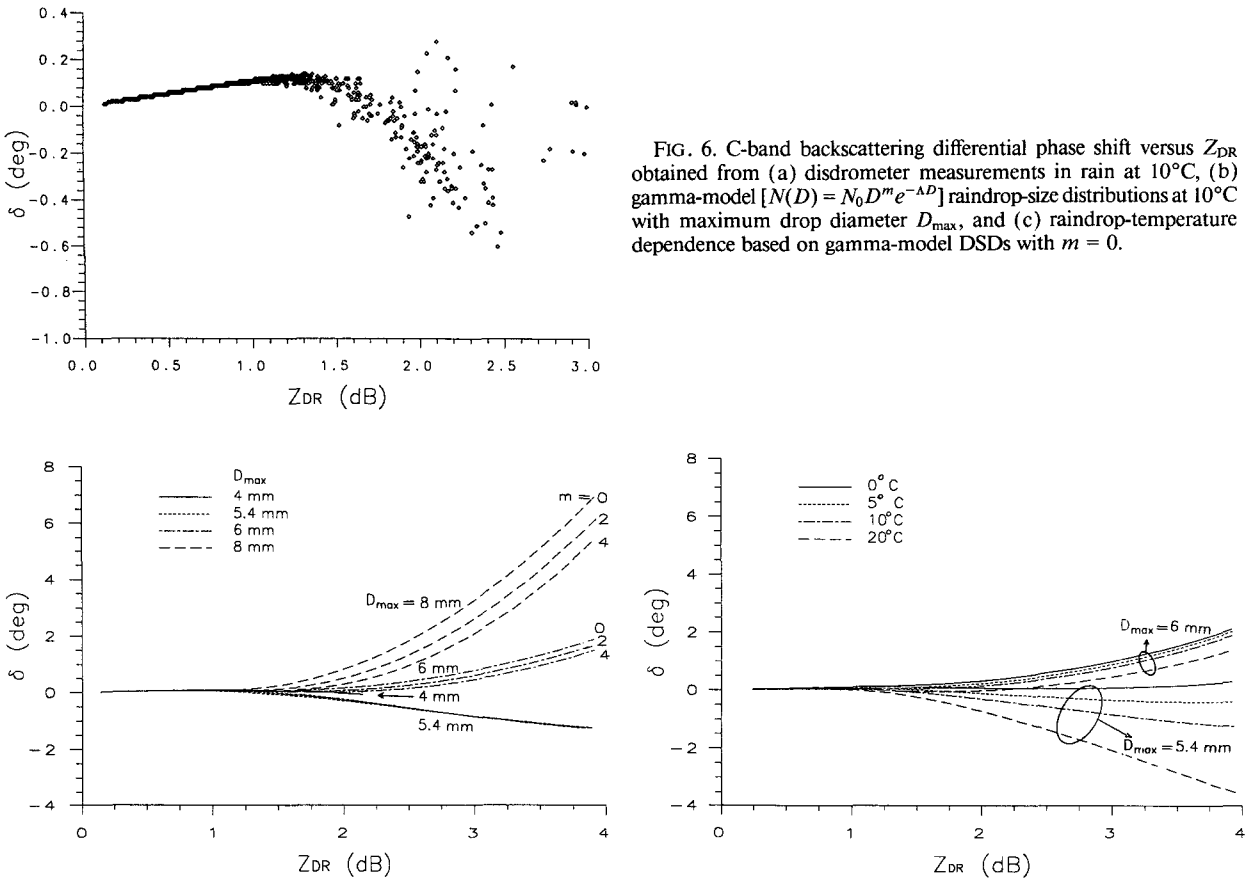

FIG. 6. C-band backscattering differential phase shift versus Z_{DR} obtained from (a) disdrometer measurements in rain at 10°C, (b) gamma-model [$N(D) = N_0 D^m e^{-\Lambda D}$] raindrop-size distributions at 10°C with maximum drop diameter D_{max}, and (c) raindrop-temperature dependence based on gamma-model DSDs with $m = 0$.

be reduced by simultaneously using several different radar observables. Also note that raindrop temperature negligibly affects the relations between these radar observables, except for ρ versus Z_{DR}, which is impacted significantly. On the other hand, raindrop canting has a minor effect on all these relations.

Relationships of R–(Z_H, Z_{DR}), R–K_{DP}, and R–Z_H were derived from disdrometer measurements for estimating rainfall rate. Among these, (Z_H, Z_{DR}) provided the best estimates of R over the range 0.5–218 mm h^{-1}, and was closely followed by K_{DP}. The R–Z_H relationship did not perform as well as the other two. The effects of raindrop temperature and canting on these relations was very small, less than 5% error in R due to temperature variations, and less 7% error due to canting. The R–Z_H relation was the least affected by canting, with less than 1% error.

A major problem for C-band radar measurements in rain is attenuation. The specific differential phase K_{DP} has been suggested for use in estimating the specific attenuation. For this purpose, relationships between K_{DP} and A_H, A_V, and ΔA_{HV} were derived from disdrometer measurements. These relations were shown to be significantly affected by raindrop temperature, leading to errors in A_H, A_V, and ΔA_{HV} ranging from 14% to 26%. On the other hand, the effects of raindrop canting was much smaller, causing errors less than 8%.

The backscattering differential phase shift δ was discussed as an error source in the estimate of K_{DP}; δ was shown to be very sensitive to the drop-size distribution and raindrop temperature.

Acknowledgments. This work was supported in part by the Army Research Office under Contract DAAL 03-89-K-0158 and by the National Science Foundation under Grant ATM 8921014.

APPENDIX

S-Band Relations

S-band (10.9-cm wavelength) relations obtained from the disdrometer data that correspond to equations (2), (3), (5), (6), (7), (8), and (9) are presented here. These results are based on 10°C raindrop temperature with a dielectric constant of 80.34-j16.87, and are not affected by temperature variations from 0° to 20°C. The rainfall boundary (2) in the Z_H–Z_{DR} plane was

originally derived at this S-band wavelength. The other equations are

$$Z_H\,(\mathrm{dBZ}) = \begin{cases} 12.53\log(K_{\mathrm{DP}}) + 48.58 \\ \qquad 0.01 < K_{\mathrm{DP}}\,(^\circ\ \mathrm{km}^{-1}) < 0.15 \\ 11.54\log(K_{\mathrm{DP}}) + 47.60 \\ \qquad 0.15 \leqslant K_{\mathrm{DP}}\,(^\circ\ \mathrm{km}^{-1}) < 7 \end{cases} \tag{A1}$$

$$Z_H\,(\mathrm{dBZ}) = \begin{cases} 0.64Z_{\mathrm{DP}} + 14.8 \\ \qquad 1 < Z_{\mathrm{DP}}\,(\mathrm{dBZ}) \leqslant 20 \\ 0.88Z_{\mathrm{DP}} + 10 \\ \qquad 20 < Z_{\mathrm{DP}}\,(\mathrm{dBZ}) < 52 \end{cases} \tag{A2}$$

$$\rho = 0.99998 - 0.00007Z_{\mathrm{DR}} - 0.00317Z_{\mathrm{DR}}^2 + 0.00080Z_{\mathrm{DR}}^3 - 0.00003Z_{\mathrm{DR}}^4. \tag{A3}$$

Equation (A1) is very similar to the relation given by Balakrishnan and Zrnić (1990), which is $Z = 13.86\log(K_{\mathrm{DP}}) + 48.17$ where Z is the average of Z_H and Z_V.

The rain-rate relations are

$$R = 2.38 \times 10^{-3} Z_H^{0.943} Z_{\mathrm{DR}}^{-1.23} \tag{A4}$$

$$R = \begin{cases} 36.15K_{\mathrm{DP}}^{0.84} & 0.01 < K_{\mathrm{DP}}\,(^\circ\ \mathrm{km}^{-1}) < 1.5 \\ 33.77K_{\mathrm{DP}}^{0.97} & 1.5 \leqslant K_{\mathrm{DP}}\,(^\circ\ \mathrm{km}^{-1}) < 7 \end{cases} \tag{A5}$$

$$R = \begin{cases} 0.08Z_H^{0.446} & 10^{1.8} < Z_H\,(\mathrm{mm}^6\ \mathrm{m}^{-3}) < 10^3 \\ 0.01Z_H^{0.749} & 10^3 \leqslant Z_H\,(\mathrm{mm}^6\ \mathrm{m}^{-3}) < 10^{5.6}. \end{cases} \tag{A6}$$

Equation (A4) is similar to the relation given by Chandrasekar et al. (1990): $R = 1.98 \times 10^{-3} Z_H^{0.97} Z_{\mathrm{DR}}^{-1.05}$, which produces higher rain rates and seems to compare better with the C-band relation (7) given in section 2b. Equation (A5) is similar to the expressions $R = 37.1K_{\mathrm{DP}}^{0.866}$ and $R = 40.5K_{\mathrm{DP}}^{0.85}$ given by Sachidananda and Zrnić (1987) and Chandrasekar et al. (1990), respectively. Equation (A5) matches better with the former equation when $R \leqslant 110$ mm h^{-1} and with the latter when $R > 110$ mm h^{-1}.

REFERENCES

Atlas, D., 1990: *Radar in Meteorology.* Amer. Meteor. Soc., 806 pp.

Aydin, K., T. A. Seliga, and V. Balaji, 1986: Remote sensing of hail with a dual linear polarization radar. *J. Climate Appl. Meteor.*, **25,** 1475–1484.

——, H. Direskeneli, and T. A. Seliga, 1987: Dual polarization radar estimation of rainfall parameters compared with ground-based disdrometer measurements: 29 October 1982, Central Illinois Experiment. *IEEE Trans. Geosci. Remote Sens.*, **GE-25,** 834–844.

——, Y. Zhao, and T. A. Seliga, 1989: Rain-induced attenuation effects on C-band dual polarization meteorological radars. *IEEE Trans. Geosci. Remote Sens.*, **25,** 57–66.

——, Y. M. Lure, and T. A. Seliga, 1990: Polarimetric radar measurements of rainfall compared with ground-based rain gauges during MAYPOLE'84. *IEEE Trans. Geosci. Remote Sens.*, **28,** 443–449.

Balakrishnan, N., and D. S. Zrnić, 1990: Estimation of rain and hail rates in mixed-phase precipitation. *J. Atmos. Sci.*, **47,** 565–583.

Bringi, V. N., V. Chandrasekar, N. Balakrishnan, and D. S. Zrnić, 1990: An examination of propagation effects in rainfall on radar measurements at microwave frequencies. *J. Atmos. Oceanic Technol.*, **7,** 829–840.

Chandrasekar, V., V. N. Bringi, N. Balaskrishnan, and D. S. Zrnić, 1990: Error structure of multiparameter radar and surface measurements of rainfall. Part III: Specific differential phase. *J. Atmos. Oceanic Technol.*, **7,** 621–629.

Golestani, Y., V. Chandrasekar, and V. N. Bringi, 1989: Intercomparison of multiparameter radar measurements. Preprints, *24th Conf. Radar Meteor.*, Tallahassee, FL, Amer. Meteor. Soc., 309–314.

Green, A. W., 1975: An approximation for the shapes of large raindrops. *J. Appl. Meteor.*, **14,** 1578–1583.

Jameson, A. R., and E. A. Mueller, 1985: Estimation of differential phase shift from sequential orthogonal linear polarization radar measurements. *J. Atmos. Oceanic Technol.*, **2,** 133–137.

Marshall, J. S., and W. Mc. K. Palmer, 1948: The distribution of raindrop with size. *J. Meteor.*, **5,** 165–166.

Ray, P. S., 1972: Broadband complex refractive indices of ice and water. *Appl. Opt.*, **11,** 1836–1844.

Sachidananda, M., and D. S. Zrnić, 1986: Differential propagation phase shift and rainfall rate estimation. *Radio Sci.*, **21,** 235–247.

——, and ——, 1987: Rain rate estimated from differential polarization measurements. *J. Atmos. Oceanic Technol.*, **4,** 588–598.

Seliga, T. A., and V. N. Bringi, 1976: Potential use of radar reflectivity measurements at orthogonal polarizations for measuring precipitation. *J. Appl. Meteor.*, **15,** 69–76.

——, K. Aydin, and H. Direskeneli, 1984: Comparison of disdrometer-derived rainfall and radar parameters with differential reflectivity radar measurements during MAYPOLE 1983. Preprints, *22nd Conf. Radar Meteor.*, Zurich, Amer. Meteor. Soc., 358–363.

——, ——, and ——, 1986: Disdrometer measurements during an intense rainfall event in central Illinois: Implications for differential reflectivity radar observations. *J. Climate Appl. Meteor.*, **25,** 835–846.

Waterman, P. C., 1969: Scattering by dielectric obstacles. *Alta. Freq.*, **38,** 348–352.